LASER INTERFEROMETER GRAVITATIONAL WAVE OBSERVATORY
- LIGO -
CALIFORNIA INSTITUTE OF TECHNOLOGY
MASSACHUSETTS INSTITUTE OF TECHNOLOGY

Technical Note	**LIGO-T1700195–v1**	2017/09/19

Mirror Metrology using Mode Spectroscopy

Kaustubh Singhi
Mentors: Koji Arai and Rana Adhikari

California Institute of Technology
LIGO Project, MS 18-34
Pasadena, CA 91125
Phone (626) 395-2129
Fax (626) 304-9834
E-mail: info@ligo.caltech.edu

Massachusetts Institute of Technology
LIGO Project, Room NW22-295
Cambridge, MA 02139
Phone (617) 253-4824
Fax (617) 253-7014
E-mail: info@ligo.mit.edu

LIGO Hanford Observatory
Route 10, Mile Marker 2
Richland, WA 99352
Phone (509) 372-8106
Fax (509) 372-8137
E-mail: info@ligo.caltech.edu

LIGO Livingston Observatory
19100 LIGO Lane
Livingston, LA 70754
Phone (225) 686-3100
Fax (225) 686-7189
E-mail: info@ligo.caltech.edu

http://www.ligo.caltech.edu/

1 Introduction

1.1 Gravitational Wave Detection

Gravitational Waves(GW) are ripples in space-time propogating at the speed of light. These were predicted on the basis of the General Theory of Relativity proposed by A. Einstein(See [1] and [2]). Detection of these GWs has always been a challenging objective as the interaction of gravity and masses is inherently weak. Therefore, it is not possible to create GWs with detectable amplitude in a laboratory wiht the current level of technoology. Hence, we look for massive and higly accelerated astronomical and cosmological systems, like binary systems formed by two compact stars such as black hole, neutron star and white dwarf, spinning compact stars, and supernovae explosions as sources for GWs. For more information, check [3]. These GWs can provide us with unique information of the Universe and its birth.

The first GW discovery by LIGO Livingston, Louisiana, and Hanford, Washington, USA on September 14, 2015, the GW150914 has opened a lot of doors for research and progress in the interferometers used for the detection. A schematic of the interferometers used for GW detection is shown in Figure 1.

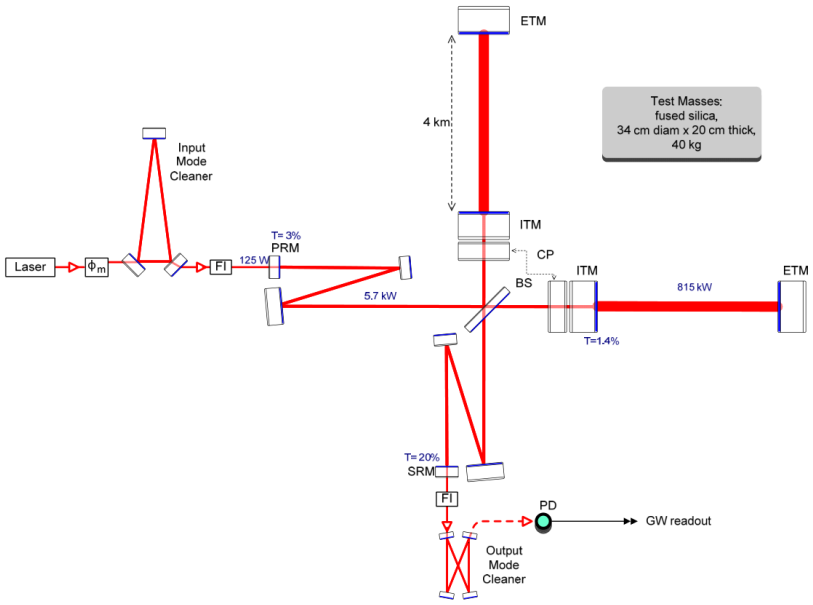

Figure 1: Michelson type Interferometer with Arm Cavities to Detect GWs.[4]

1.2 Impact of Mirror Figure Error on Detector Perfomance

The LIGO Fabry-Pérot Michelson interferometers consist of multiple optical cavities, and hence multiple mirrors. Now these mirrors are not *perfect*, and hence have some imperfections such as point defects, absorption losses, coating losses, contamination, etc. One such defect is the ***mirror figure error***. The mirror figure error is a *low spatial frequency* surface defect present on the test masses, which causes low angle *scattering* of light. The primary

objective of this project is to develop an *in-situ* technique for the measurement of the mirror figure error. Due to these mirror imperfections, there are *optical losses* involved with the cavities. As depicted in the following diagram, these optical losses result in a reduced total circulating power inside the cavity arms and the destruction of the squeezzed state of light, both of which, in turn cause an apparent rise in the **shot noise GW output**.

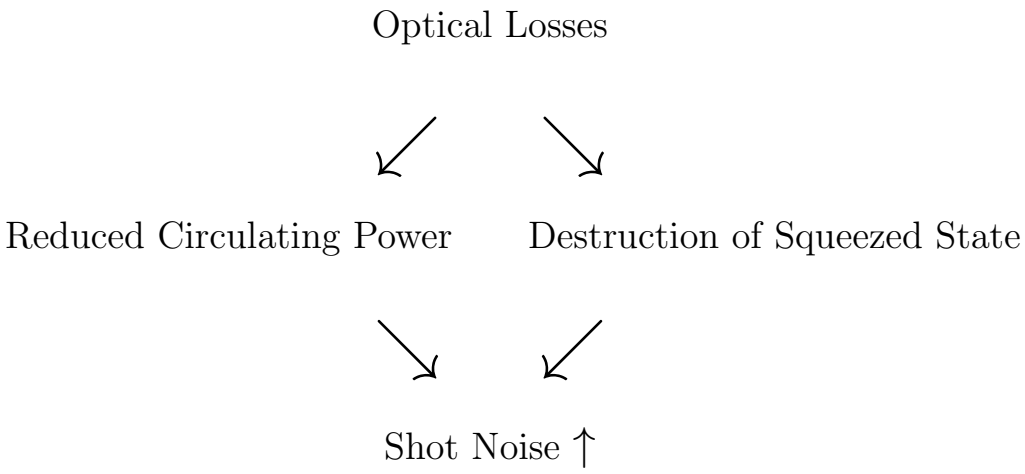

1.3 Requirement of an *In-Situ* Measurement Technique

We often characterize the mirror surface defects using *phase/mirror maps* like the one shown in Figure 2. Phase maps such as these are conventionally produced using techniques such as Fizeau interferometry[5].

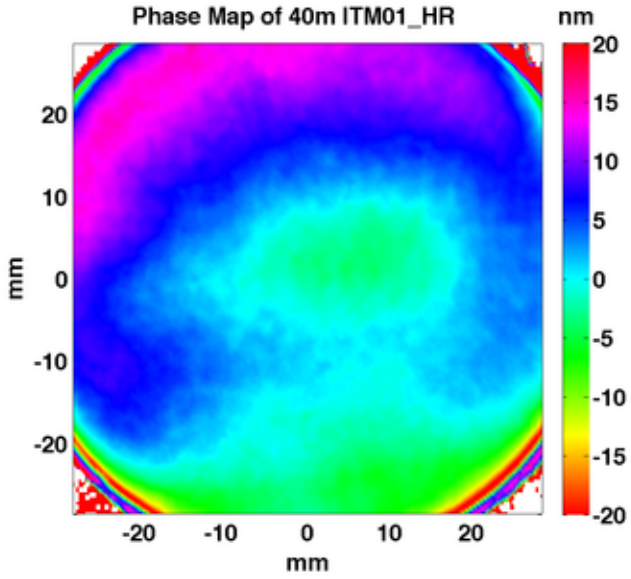

Figure 2: Phase Map of ITM surface using Fizeau interferometry

If possible, we would like to develop a technique to produce high resolution mirror maps for the test masses. This technique should use the actual laser in the interferometer so that

we can also specify which region of the mirror map is contributing towards the loss. Also, we would like to produce a mirror map using a cavity interferometer of high sensitivity, like the LIGO interferometers. Hence, we would like to have an *in-situ* measurement technique for producing mirror maps. The in-situ technique that we have employed in this project is called **Mode Spectroscopy**.

2 Mode Spectroscopy

2.1 Properties of an Optical Resonator

There can be various kinds of optical resonators, charecterized by the radii of curvartures of the mirrors of the resonator and the absolute distance between them. An optical resonator has, inturn, a certain set of *Hermite-Gaussian modes* which are allowed to resonate inside it. Using the eigen *H-G modes*, we can construct any kind of laser signal, i.e. a laser with some *'dirty'* modes present in it can be expressed as a linear combination of these eigenmodes. Now, depending upon the charecterizing paramaters of a resonator and the frequency of the laser, only **certain modes** will be allowed to **resonate** inside it. This allows the resonator to act as a ***filter*** for the laser.

The 40m as well as the aLIGO interferometers have Fabry Pérot resonators composed of ITMs and the ETMs.. An important characteristic of the Fabry Pérot cavity is that the transmittance of the two mirrors is extremely small($\approx$15 ppm[†]) and the reflectance is high($\approx$1). This allows us to differentiate between the frequencies of light that have a round trip phase difference as a multiple of 2π from other frequencies. This is discussed in more detail in section 2.2

The Free Spectral Range(FSR) of a Fabry-Pérot Cavity is defined as the spacing in frequency between two resonant longitudinal modes and is denoted by f_{FSR} in the figure. The HOMs are not shown in the plot but they too occur with the same period of f_{FSR} as the fundamental TEM_{00} mode. Another quantity used to characterize an optical cavity is the Transverse Mode Spacing(TMS) and it is defined as the spacing in frequency between transverse modes. Both the FSR and the TMS are uniquely determined by the defining parameters of an optial cavity, i.e. the absolute length between the mirrors and the radii of curvature of the two mirrors. Section 3 discusses some techniques for measuring these quantities.

2.2 Simulated 40m Fabry-Pérot Cavity

We will be analyzing the transmission plot for the 40m cavity. We perform a *cavity scan* to obtain such a plot for the actual cavity. In this section we will see how such a transmission plot would look like. The cavity equations, along with the relevant cavity parameters that we require to simulate or analyze a scan have been described in Appendix B. Using the values in table 1 as the ***ideal*** mirror parameters and taking the cavity length, $L = 40m$, a simulated transmission plot is shown in figure 3

[†]These values are for the 40m.

Table 1: Mirror Parameters

Parameter	M_1	M_2
RoC	$R_1 = \infty$	$R_2 = 60m$
Reflectivity	$r_1 = \sqrt{0.986}$	$r_2 = \sqrt{0.999985}$
Transmissivity	$t_1 = \sqrt{0.014}$	$t_2 = \sqrt{0.000015}$

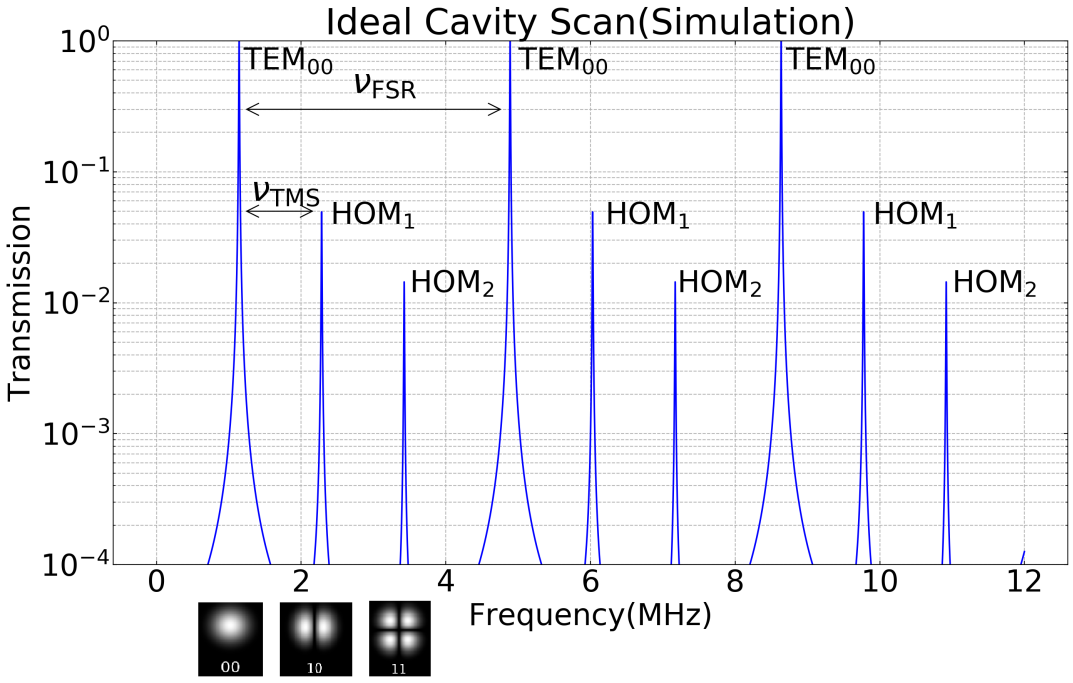

Figure 3: Transmission Intensity variation with Laser Frequency for an FP Cavity

This cavity is similar to the main interferometer arm used in the 40m interferometer. For the simulation, I have assumed that the laser is perfectly mode matched into the cavity. I have considered that the laser itself consists of the fundamental mode and the first two higher order modes, i.e., TEM_{nm}, for $n + m = 0, 1, 2$. The FSR and TMS frequencies have been shown in the plot. These are as follows:

$$\nu_{\text{FSR}} = \frac{c}{2L} \approx 3.74MHz$$

$$\nu_{\text{TMS}} = \frac{\nu_{FSR}}{\pi} \times \arccos\sqrt{g_1 g_2} \approx 1.14MHz$$

2.3 Deviation of the Higer Order Modes from the equal spacing

Now that we have seen an *ideally* simulated cavity scan, let's try and get a sense of how the mirror figure error error will affect this scan. The figure error can be simply treated a *perturbation* on the surface of the mirror. This suggests that we can account for the figure

error by modifying the resonant frequencies for the eigen H-G modes inside the cavity. The figure error will affect each H-G mode in a different manner, i.e. it will cause a ***shift*** in the corresponding resonant frequency for that mode. Depending apon how the figure error varies over the surface of the mirror, this shift will be different for each mode. The overall plot would still remain periodic with a period of ν_{FSR}. The figure error in our mirrors is assumed to be small, implying that the expected shift in each mode would not be a lot. An extremely exaggerated version of the effect of figure error on the transmission plot in figure 3 is depicted in figure 4.

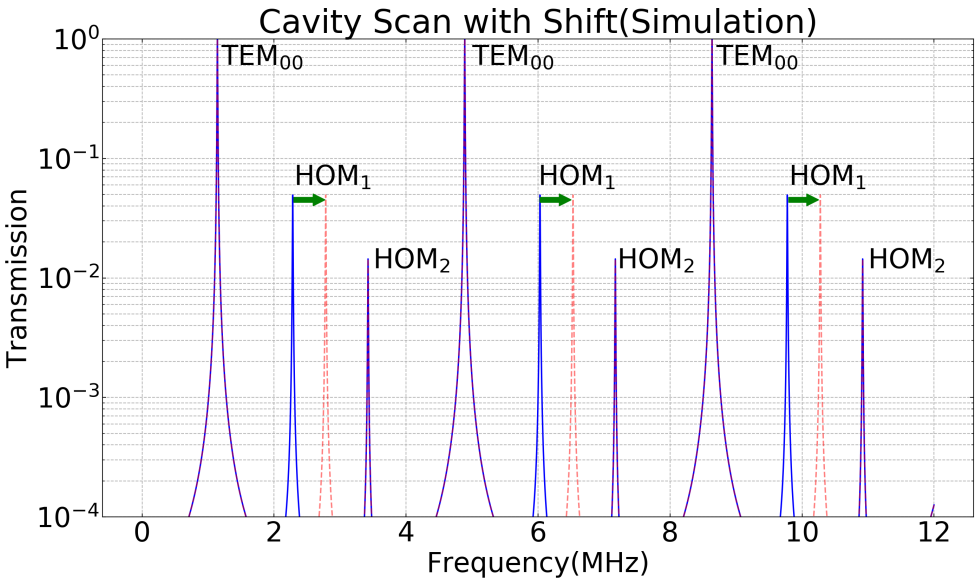

Figure 4: Over-exaggerated Shift in HOM_1 Resonant Frequency

Using the mirror maps we already have(using other methods), we can provide a certain bound over the figure error and assure ourselves that the mirror figure error would not cause a *large* shift in the TMS values.

3 Experimental Methods

3.1 Cavity Scan

In principle, a *cavity scan* is simply sweeping the laser frequency and obtaining a transmission plot for the sweep. So, in an **ideally stable** system, a simple setup like the one shown in figure 5 should work.
Once we have the transmission scan, we can identify the various HOMs and fit it with the FP cavity equations in order to obtain the respective shifts in the resonant frequncies.

Perform a Cavity Scan and Obtain a Transmission Plot

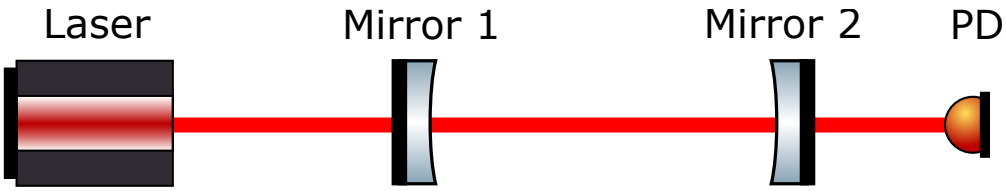

Figure 5: Simple Cavity Scan Setup

↓

Identify the HOMs

↓

Perform a Fit and Determine the Relative Shifts in Resonant Frequencies

This kind of a setup would only work in an ideally stable system, i.e., a system free of any disturbances that might cause the mirrors to move. Unless externally controlled, it is impractical to leave the cavity on its own while we perform the laser sweep and expect the cavity to be stable throughout the this sweep. Hence we use other techniques to obtain a transmission scan for the cavity.

3.2 Using an EOM

In this method, for a given carrier frequency, we generate *'sideband'* frequencies using an Electric Optical Modulator(EOM), as shown in figure 6 and 7. We then bring the main laser in resonance with the cavity and start varying the sideband RF frequency. We obtain the transmission plot as we vary the sideband frequency. This technique has been used to determine the FSR([6]) and TMS([7]) values using high-finesse Fabry-Pérot interferometers.

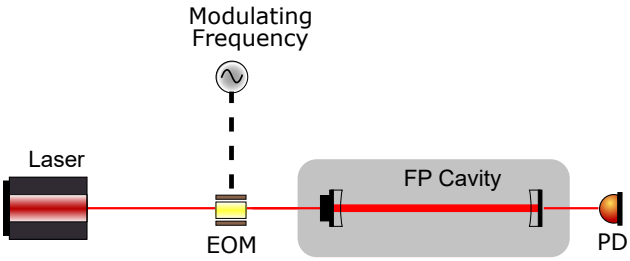

Figure 6: Using an EOM to generate sideband frequencies

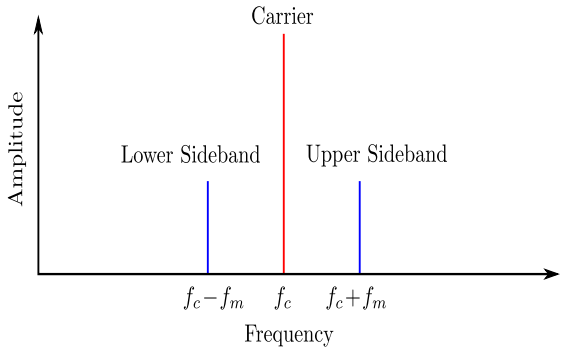

Figure 7: The carrier and sideband frequncies.

3.3 Using an Additional Slave Laser

The setup for this technique is as shown in figure 8. In this technique, we add an additional *'slave'* laser(Laser 2 in figure) along with our *'master'* laser(Laser 1 in figure). This slave laser is offset in frequency from the master laser set by a *local oscillator*(LO). The Phase Locked Loop(PLL) ensures that the relative frequency of the two lasers remains constant. Both the lasers are injected into the cavity and then the cavity is locked with the master laser's fundamental mode in resonance using the Pound-Drever-Hall technique[8]. After transmission from the cavity, the RF photodiode at the end detects the intensity of the beat note between the two lasers. Now, in order to perform a cavity scan, we vary the laser offset using the LO while the cavity is held stable in resonance with the master laser, and obtain the transmission intensity using a spectrum analyzer connected to the photodiode. The technique is described in more detail in Alberto's paper[9].

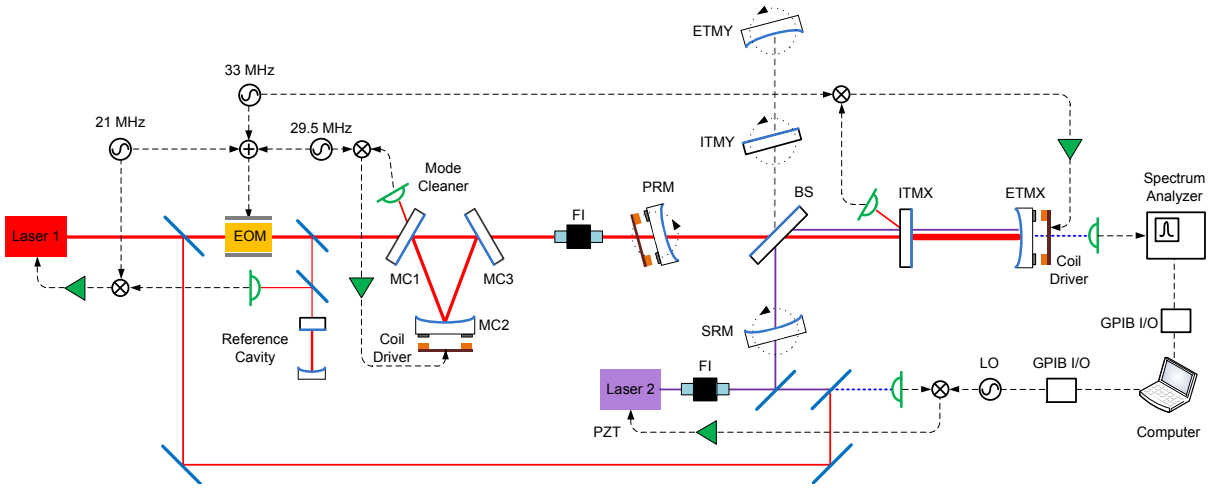

Figure 8: Cavity Scan using an Additional Slave Laser

3.4 Arm Length Stabilization(ALS) Scheme

The schematic for the ALS scheme used in the 40m lab is shown in figure 9. In this technique too we use an additional *auxiliary* laser along with the main pre stabilized laser(PSL). This Aux laser(1064 nm) is fed to a KDP crystal and goes through a non-linear optical process called Second Harmonic Genration(SHG)([10] and [11]). In this process the laser frequency gets exactly doubled(wavelength gets halved) and hence the output from this crystal is of wavelength 532nm(green in colour). Now this *green* beam is incident on the main interferometer arm from the *'back'* side, i.e. from the end test mass(ETM). Also, a part of the PSL is taken aside(as seen in the schematic) and passed through another KDP crystal too obtain another green beam. Now the this beam and the green beam coming through the input test mass(ITM) side of the cavity, corresponding to the Aux laser are made incident on a RF photodiode connected to a delay-line frequency discriminator. The frequency discriminator then feeds this data to the arm length control system to stabilize the cavity. The Aux control system is programmed such that the Aux laser *'follows'* the cavity length, i.e. its frequency is modulated such that it is **always** resonant inside the cavity. We

can provide the arm length control system with a **frequency offset**, which is simply the beat note between the second harmonics of the PSL and the Aux laser. As we vary the offset, the arm length changes, and sequentially, so does the Aux laser frequency. Now using the frequency discriminator, we can obtain the beat frequency data along with the transmission intensity of the PSL. The ALS scheme, particularly for the 40m, is described in much more detail in Izumi's paper[12].
Note: The delay-line frequency discriminator has some non-linear characteristic which limits the precision of the scan.

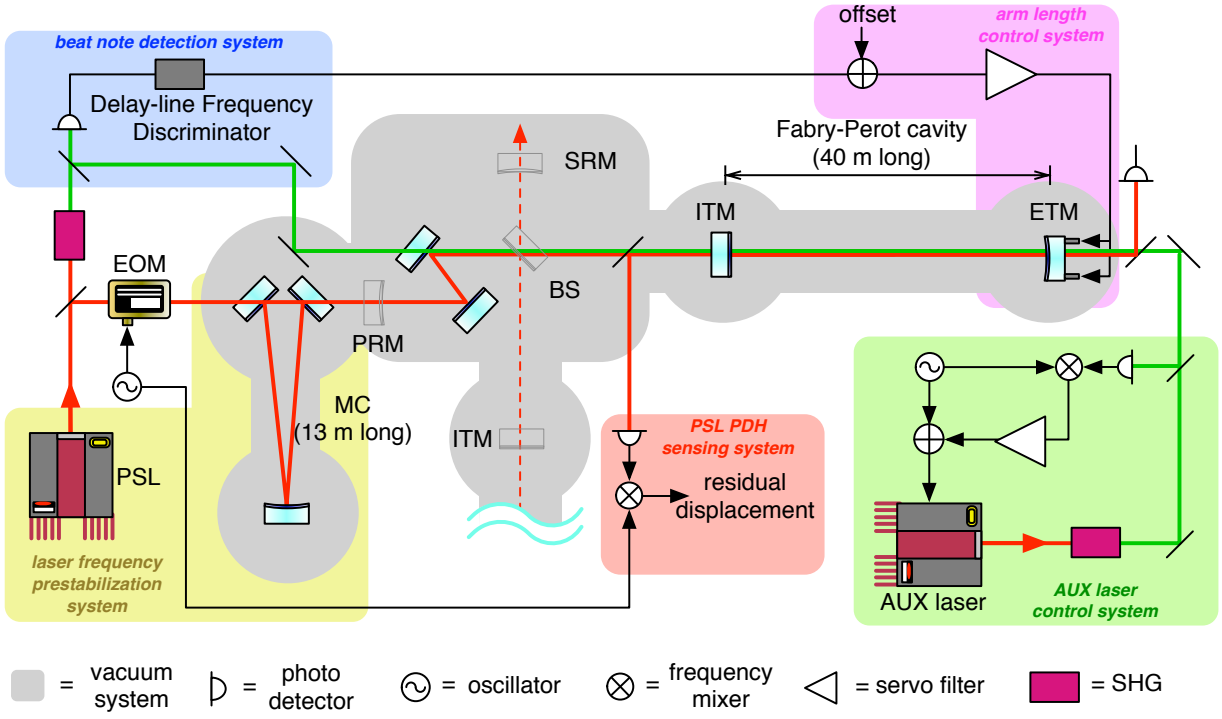

Figure 9: Arm Length Stabilization Scheme for the 40m

4 Experiment Report and Result

4.1 Cavity Scan Data

Now that we have discussed the various techniques that can be used to obtain a cavity scan, we can look at actual data from a cavity scan. Figure 10 corresponds to a cavity scan taken using the Arm Length Stabilization technique in the 40m interferometer. It is easy to see that there are certain *peak resonances* in the scan. These peaks correspond to the fundamental as well as the higher order modes(HOMs). There are some other peaks present corresponding to the sideband resonances of 11 MHz and 55 MHz.

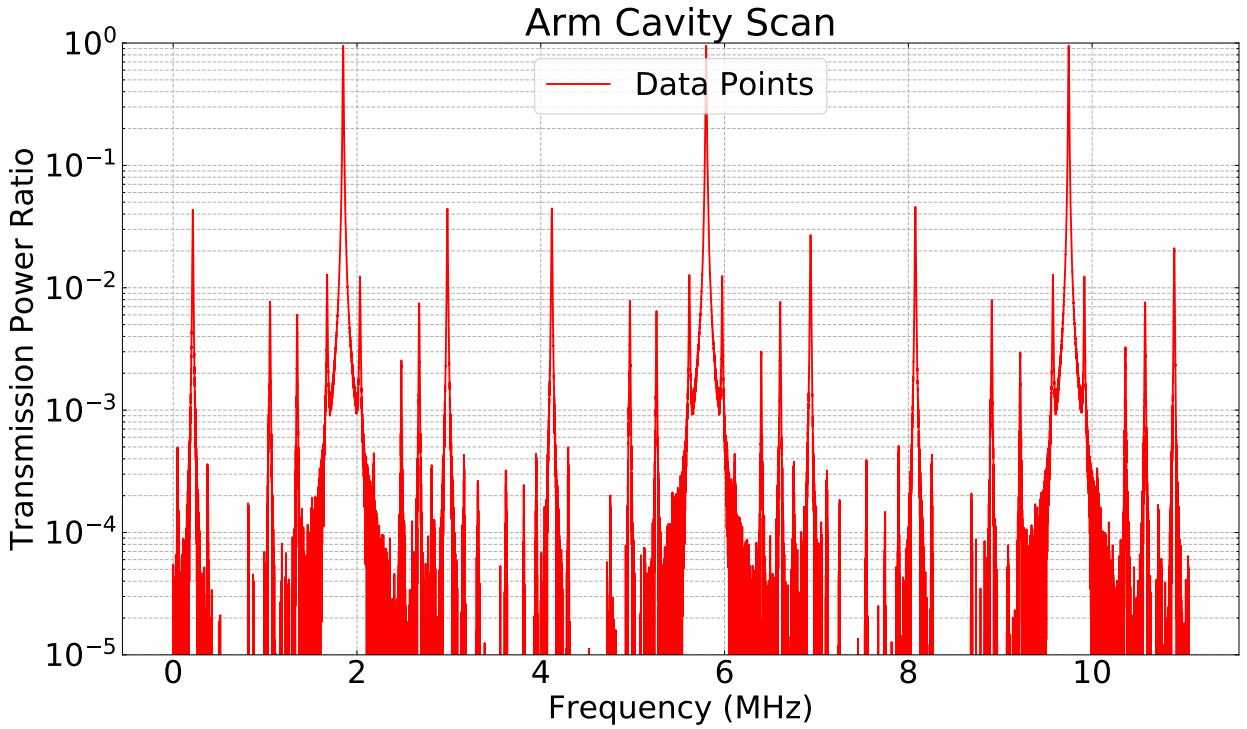

Figure 10: Raw Cavity Scan Data for the 40m.

4.2 Fitting Process to Evaluate the Cavity Scan Data

In order to evaluate the scan and determine some meaningful parameters(such as the free spectral range(ν_{FSR}), Finesse, transverse mode spacing(ν_{TMS})), we perform a fit on the scan data. For this purpose we use the Fabry-Pérot cavity equations, as stated in the appendix B, as our fitting model. But, instead of using these equations directly, we reduce the transmission to a *Lorentzian* function in frequency **around the peaks**. The details on the approximation of the cavity equations using a Lorentzian distribution is explained in appendix C. Now, the fitting has to be performed on each indivdual peak resonance and then add the resulatant Lorentzian distributions to obtain a 'fit' for the entire scan data. The code to perform the fitting process and then evaluate the *parameters* can be found at [17].

4.2.1 Peak Identification

In order to perform the fit on the individual peak resonances, we first need to find a ***neat*** way to ***identify*** them first. One can easily find the resonant peaks using some standard functions/modules such as the *'peakutils'* module for Python. After finding the peaks we need to identify each of them. For this, we use some prior knowledge we have about the cavity parameters. Also, as we know that most of the laser power is contained in the fundamental mode, we can directly identify the maximum transmission power peaks as the fundamental resonances. The values stated in table 1 and the cavity length help us determine the *rough* values for ν_{FSR} and ν_{TMS}. We know that the sideband resonances are 11 MHz and 55 MHz *away* from the fundamental resonances. Studying this *modulo* the ν_{FSR}, we can identify

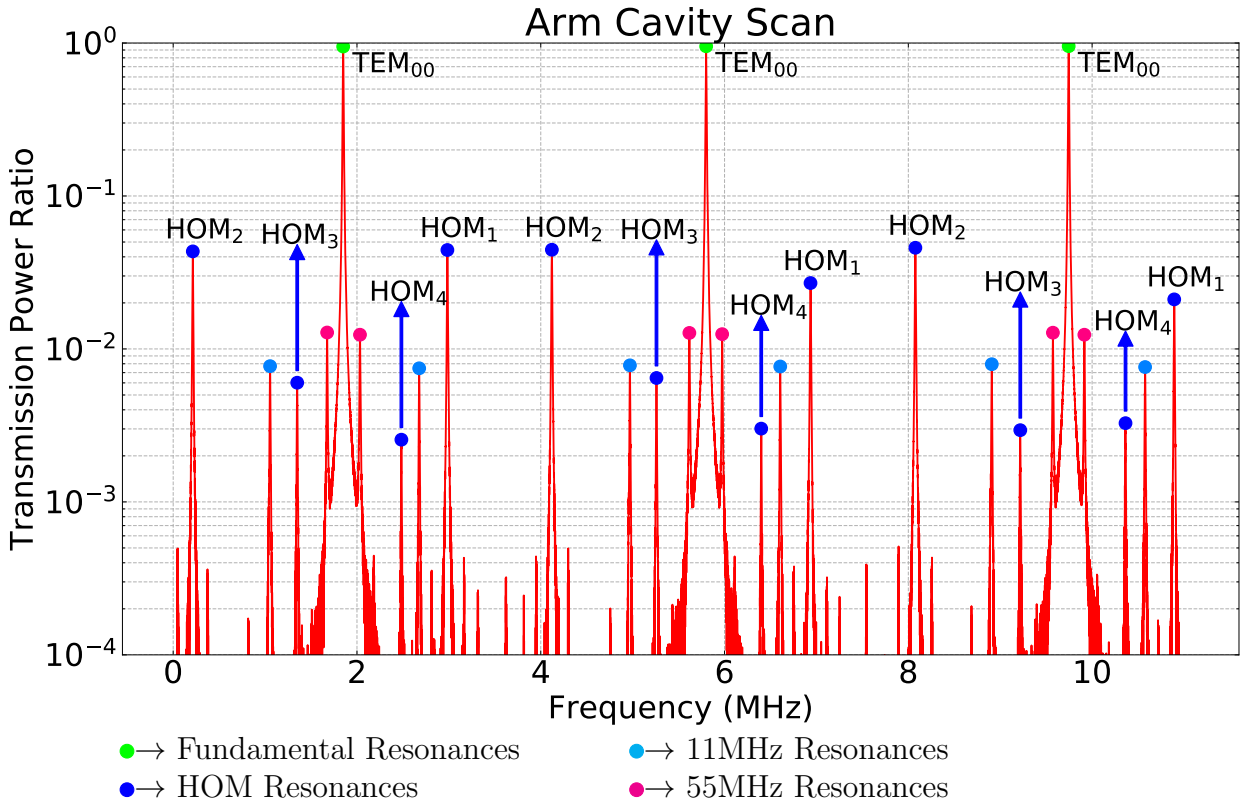

Figure 11: Identified Peaks in the Cavity Scan Data

the sideband resonances as well. Now, the remaining peaks belong to the higher order modes(HOMs). In order to identify these, we study how *far* these are from the fundamental resonances and compare the values with the ν_{TMS} value to identify the order$(n+m)$ of the HOM. Figure 11 shows the identified peaks.

4.2.2 Fit and Residuals

Once we have identified all the peaks, we can proceed with fitting each of them with the Lorentzian model we are using to approximate the cavity equations. This approximation is only valid in a ***small*** interval about the peak resonance. The different Lorentzian functions we obtain through fitting correspond to each peak and drops down to an *extremely small*† value near other peaks. Hence, in order to reconstruct the cavity scan data, we add each of the Lorentzians and obtain an overall *'fit'* for the scan data. The final fit along with the residuals is shown in figure 12.

†Subject to the limitation of the Lorentzian approximation.

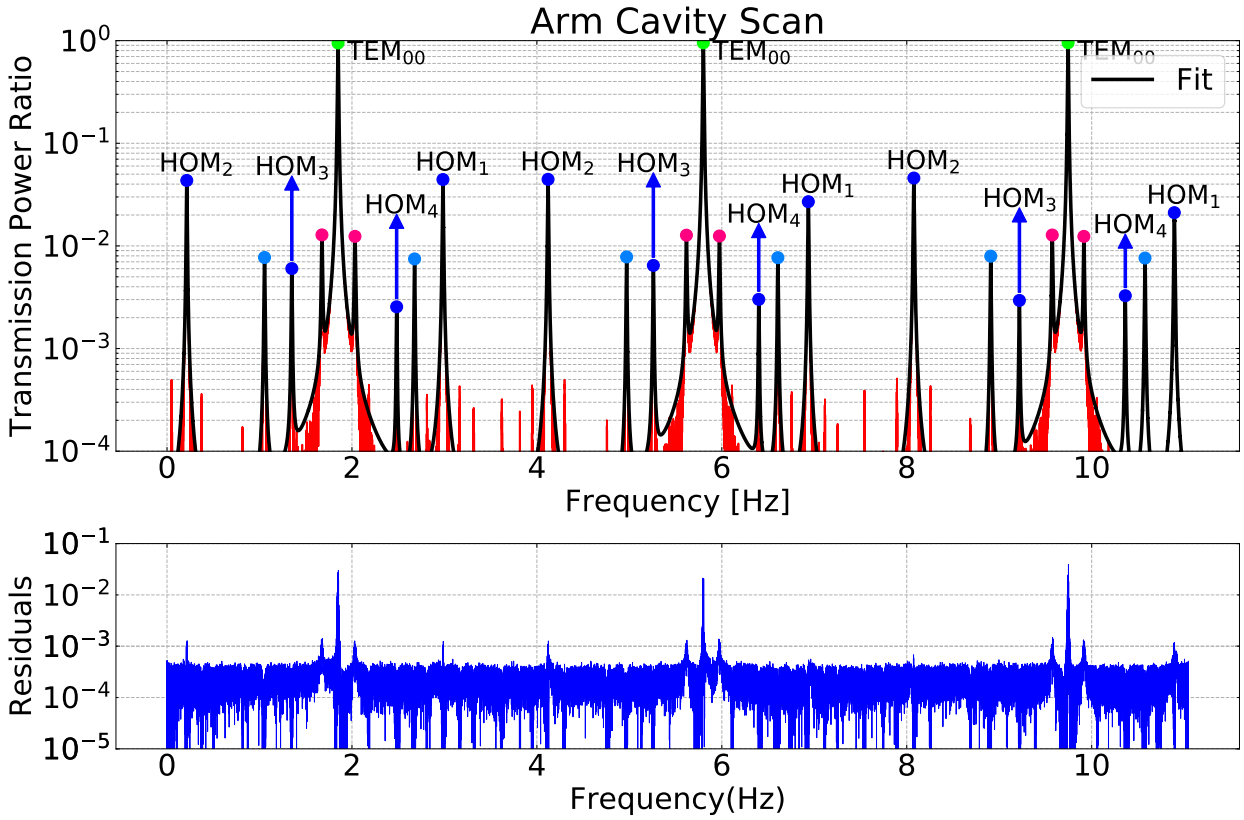

Figure 12: Fit and Residuals for the Cavity Scan Data

4.3 Parameter Determination

4.3.1 Free Spectral Range and Finesse

Now that we have performed the fit on the cavity scan data using a *Lorentzian* fitting model, we can obtain the physically relevant parameters, viz. $\nu_{\text{FSR}}/\textit{Cavity Length}$, *finesse* and ν_{TMS} from the fit parameters($'a'$, $'b'$ and ν_0). The relations/equations shown in appendices B and C are used to determine the parameters as follows:

1. For ν_{FSR} - The Free Spectral Range, by definition, is simply the *periodicity* in the cavity scan data, i.e. it is simply the difference in frequencies between two i^{th} order resonances. But because our system isn't ***ideal***, the resonances aren't *perfectly* periodic. Therefore we consider the *average*† of the different values. The resulting FSR and Cavity Length are:

$$\text{FSR, } \nu_{\text{FSR}} = 3.9703 \pm 0.00022 \text{ MHz}$$

$$\text{Cavity Length, } L = 37.754 \pm 0.00207 \text{ m}$$

Note: The error shown here is only due to the fitting procedure. We are actually limited in precision and accuracy because of the delay-line frequency discriminator due its non-linear characteristics.

†The average is/can be weighted.

2. For $\mathcal{F}$ - The Finesse is related to the ***linewidth*** parameter($'b'$)[†] as:

$$\mathcal{F} = \frac{\nu_{\text{FSR}}}{2b}$$

Again, we need to take an *average*[††] of the different finesse values obtained using the corresponding FSR and $'b'$ values. The resulting Finesse is:

$$\text{Finesse}, \ = 402 \pm 21$$

4.3.2 TMS Shifts

We have the *fit parameters* corresponding to each of the higher order mode(HOM) resonances. Now, in an ***ideal*** cavity with ***perfectly*** spherical mirrors, the higher order modes are *linearly* spaced(appendix B). But, in reality the HOM peaks would be ***shifted***, not just due to the *statistical error* in measurement, but also due to the presence of the **mirror figure error** on the mirror surfaces. Therefore, we perform a *linear fit*[‡‡] on the resonant frequencies for the different HOM resonances and see the corresponding ***residuals*** to determine the **relative shifts** in resonant frequencies for the HOMs. The result is shown in figure 13.

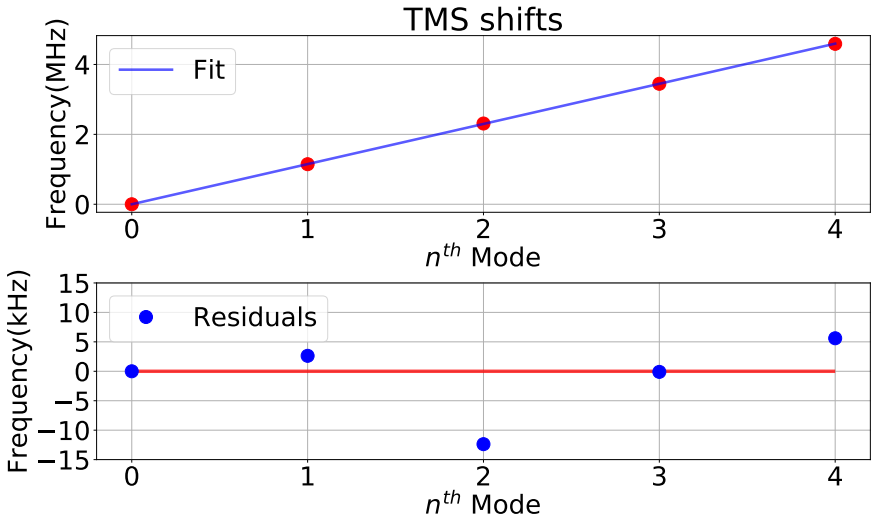

Figure 13: Relative Shifts in resonant frequencies for HOMs

4.4 Inference and Discussion of the Result

We started off saying that the mirror figure error affects the cavity scan data by influencing, or rather *shifting* the resonant frequencies for the different modes. Now that we have seen

[†]Linewidth is usually defined as the Full Width at Half Maximum(FWHM), but here we are considering only Half Width at Half Maximum(HWHM) as the linewidth, $'b'$.

[††]The average is/can be weighted.

[‡‡]The averages for each set of resonant HOM modes was considered.

an actual cavity scan, a question arises, that with respect to what are we going to determine the *'shifts'*. This is important to discuss because, while accounting for the mirror figure error, we **don't have** an ideal cavity scan to compare the actual one with. It might be a bit hard to fathom, but in other words, the physically relevant parameters like FSR and TMS are only defined for *ideal cavities* and it can prove to be quite challenging and even more confusing to define it for the actual cavity. Hence, while evaluating the cavity scan data, we don't consider the resonant frequencies for HOMs to be shifted with respect to those in an ideal cavity scan. Instead we determine the relative shifts with respect to the *linear fit* of the resonant frequencies. This, of course, corresponds to the ***least shift***(so to say) and might not be the ***correct/right*** estimate for it, but it cetainly can give us an idea of the extent of figure error.

Now, coming to the actual result obtained for the reative shifts in the TMS values seen in figure 13. Although quite a lot of further analysis is required to actually comment on this observation and make further logical inferences, a quick look at the figure shows that the *second* HOM is relatively shifted by more than **10 kHz** whereas the other HOMs are within a 5 kHz range from the *fit data*. Although there is a possibility that this is simply beacause of statistical and systematic errors and only more such observations and further detailed analysis would help us deduce as to what is the actual cause behind such an *'anomaly'*, this shift of 10 kHz certainly looks quite large compared to the others. It is quite possible that this shift is actually present due to the figure error. If that is actually the case, the next step would involve relating the figure error to the cavity scan. There is no such direct one-to-one correspondance between the figure error and the shift in the resonant frequencies, and hence, we woud need to develop another mechanism to relate the two. Section 5 would discuss more on this regard.

5 Future Prospects

Strictly speaking, this project is still *incomplete* and a lot of things can still be explored regarding it. A few of them are:

1. We would like to improve our measurement, i.e. have a more accurate and precise cavity scan data which we can trust more reliably. One of the things that can be done to improve the measurement is to use the **frequency counter** along with the delay-line frequency discriminator. This will hopefully provide us with a better precision in frequency.

2. In order to relate the mirror figure error to the shifts observed in the cavity scan for the HOMs, we can use a software called FINESSE([13]) to simulate the effects figure error causes on the cavity scan data. It allows us to customize the mirror defects to our need using *Zernike polynomials*([14]) and then generate a corresponding cavity scan. This simple mechanism allows us to iteratively simulate various different kinds of figure errors and repetitively generate cavity scans corresponding to these figure errors. Using the **Markov Chain Monte Carlo(MCMC)**([15]) method, we can try and obtain good and high resolution mirror maps. This has been explored more by Naomi in her SURF project([16]).

6 Acknowledgements

I have had a wonderful oppurtunity this summer to work alongside some really brilliant personalities. For providing me with such an exquisite experience, I would like to thank the LIGO Scientific Collaboration, the National Science Foundation, the Caltech SFP, IndIGO and the Kavli Foundation.
I would like to thank my two mentors, Koji and Rana, who are two of the smartest and wisest people I've met and have guided me throughout my 11-week stay, not just in the aspect of scientific research, but otherwise as well. Not to steal from Rana's Thesis, but I would like to thank you for all the free food and discussions on topics as bizarre as "Neil deGrasse Tyson". I really appreciate you showing us *the integrity and the passion with which science and 'fitting' should be done.*
I would like to thank all other members of LIGO-CIT and the 40m, especially Alex and Alan who planned out the whole stay for us and arranged some really amazing presentations, talks and most of all, free food for us.
I would especially like to thank Gautam, who acted as a guide for me during my entire 11-week stay and helped me with almost everything.
I would like to extend my thanks to my co-SURFers: Vineeth, Dhruva, Jigyasa, Naomi and everyone else who accompanied me.
Lastly, I would like to thank my parents and my sister who encouraged me and supported me throughout the summer program.

Appendices

A Higher Order Modes described by Hermite-Gaussian Polynomials

We know that the Higher Order Modes(HOMs) that can stably resonate in an optical cavity are described by the Hermite-Gaussian Polynomials for paraxial approximation. The general Electric field distribution in rectangular co-ordinates is given as:

$$E_{nm}(x,y,z) = E_0 \frac{w_0}{w(z)} H_n\left(\frac{\sqrt{2}x}{w(z)}\right) H_m\left(\frac{\sqrt{2}y}{w(z)}\right) \exp\left(-\frac{x^2+y^2}{w(z)^2}\right) \exp\left(-\mathrm{i}\left[kz - (1+n+m)\arctan\left(\frac{z}{z_\mathrm{R}}\right) + \frac{k(x^2+y^2)}{2R(z)}\right]\right)$$

where E_0 is the peak amplitude, $w_0, w(z)$ are the beam radius at the waist and at point 'z' on the axis, H_n represents the n^{th} order Hermite polynomial, k is the wavenumber of the light($= 2\pi/\lambda$), z_R is the Rayleigh length and $R(z)$ is the radius of curvature of the wavefronts. For the details on the derivation of these Higher Order Modes, refer to [23]. Figure 14 shows how the first few TEMs appear.

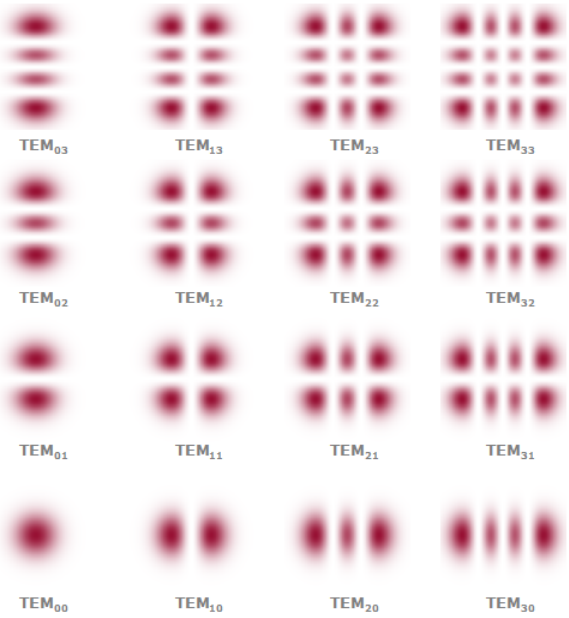

Figure 14: Intensity profiles of the lowest-order HermiteGaussian modes.[24]

B A Simple Fabry Pérot Cavity

An ideal Fabry-Pérot Cavity, where-in the mirrors are assumed to be spherical, is shown in Figure 15. These modes are obtained for different combinations of the parameters involved witht he cavity and the laser, such as the frequency of the laser, the distance between the two mirrors(arm length) and the radii of curvature of the two mirrors.

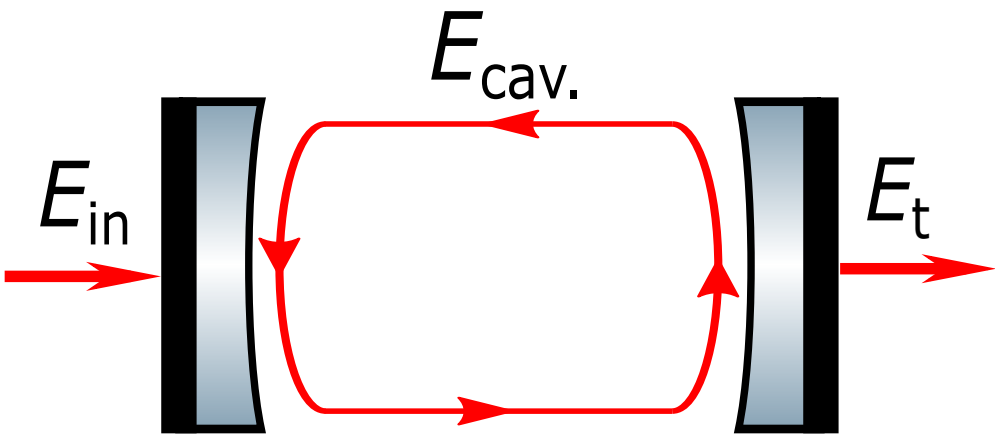

Figure 15: Schematic of a simple Fabry-Pérot Cavity

The electric fields are given as follows:

$$E_{\text{cav.}} = \frac{t_1}{1 - r_1 r_2 e^{-\mathrm{i}\phi_{\text{RT}}}} E_{\text{in}} \tag{1}$$

$$E_{\text{r}} = \left(-r_1 + \frac{r_2 t_1^2 e^{-\mathrm{i}\phi_{\text{RT}}}}{1 - r_1 r_2 e^{-\mathrm{i}\phi_{\text{RT}}}} \right) E_{\text{in}} \tag{2}$$

$$E_{\text{t}} = t_2 E_{\text{cav.}} \tag{3}$$

where E_{in}, E_{r}, $E_{\text{cav.}}$ and E_{t} are the incident, reflected, intra-cavity and transmitted electric fields respectively. The reflectivity and transmissivity of the two mirrors M_1 and M_2 are given by r_1, t_1 and r_2, t_2 respectively and ϕ_{RT} is the 'round trip' phase difference that the beam undergoes inside the cavity. The round trip phase difference distinctly depends upon the laser frequency and the TEM mode as follows:

$$\phi_{\text{RT}} = \frac{4\pi\nu \text{L}}{c} - 2N\phi_{\text{G}} \tag{4}$$

$$\text{with, } N = n + m + 1 \tag{5}$$

where $'n'$ and $'m'$ represent the TEM_{nm} mode, ν is the laser frequency, L is the absolute length between the two mirrors, c is the speed of light in the medium and ϕ_G is the *Gouy Phase Shift*. The Gouy phase is given by the charecteristic cavity parameters, L and the radii of curvatures of the two mirrors, R_1 and R_2, as follows:

$$\phi_{\text{G}} = \arccos \sqrt{g_1 g_2}$$

where g_1 and g_2 are the g-factors of the two mirrors, given as:

$$g_1 = 1 - \text{L}/R_1 \qquad \text{and} \qquad g_2 = 1 - \text{L}/R_2$$

For the derivation and the physical implication and meaning of the *Gouy Phase Shift*, refer to [23]. F-P cavities are usually made so that the transmittance of each mirror is low($\sim 10^{-3}$) and the reflectance is high(≈ 1). Putting these in the cavity equations and then analysing them will tell us that the ratio of transmission power($\propto |E_t|^2$) to that of incident power($\propto |E_{in}|^2$) is extremely small when ϕ_{RT} is not close to an integer multiple of 2π. On the other hand, whenever ϕ_{RT} is an integer multiple of 2π, almost all power is transmitted. This condition, where the round trip phase change is a multiple of 2π, is known as resonance. Now, as ϕ_{RT} is a function of both frequency and the $'n'$, $'m'$ values of TEM_{nm} mode, the resonances are determined by both of these values. This gives rise to a few defintioning parameters for an F-P cavity. These are as follows:

1. Free Spectral Range(FSR) - The FSR is defined as the frequency spacing between two consecutive resonances of the fundamental, or any higher order mode. This simply means that the ϕ_{RT} for the higher frequency is greater than that for the lower frequency by 2π. By simply using the defination and equation 4 we can see that for a change(increase/decrease) in phase by 2π, the corresponding change in the frequency, which in turn is the FSR, is $\frac{c}{2L}$.

2. Transverse Mode Spacing(TMS) - The TMS is defined as the frequency spacing between two consecutive resonances between the different modes. This would mean a change of 1 in equation 5 which can be either due to change in $'n'$ or $'m'$. As there is absolute symmetry between $'n'$ and $'m'$, this causes degeneracy in the higher order modes as several different values(simple counting mechanism will tell how many) of $'n'$ and $'m'$ might correspond to the same value of $'N'$ and in turn the same value of frequency. Now for a change of $'1'$ in the value of $'N'$, equation 4 will give us the TMS to be:

$$\nu_{TMS} = \frac{c}{2\pi L} \times \phi_G \tag{6}$$

   or better expressed as

$$\nu_{TMS} = \frac{\nu_{FSR}}{\pi} \times \arccos(\sqrt{g_1 g_2}) \tag{7}$$

   For the above formulation of the TMS, refer to [23].

3. Finesse($\mathcal{F}$) - Finesse is 'mathematically' given by the following relationship:

$$\mathcal{F} = \frac{\pi\sqrt{r_1 r_2}}{1 - r_1 r_2}$$

   where r_1 and r_2 are respectively the reflectivities of the two mirrors M_1 and M_2. Physically speaking, it denotes the 'sharpness' in the resonances of the different modes. It is directly related to the full width at half maxima of the power ratio, or 'linewidth' as follows:

$$\nu_{FWHM} = \frac{\nu_{FSR}}{\mathcal{F}}$$

   Higher the Finesse, steeper and sharper is the resonance of the modes. High Finesse helps in better identification of the peak resonant frequencies in a cavity scan.

C Fitting Model

Using the cavity equations 1 and 3 described in appendix B, and using the dact that the laser intensity/power is proportional to the elctric fied magnitude($P \propto |E|^2$) we can write the ratio of the transmision power intensity to the incident power intensity as:

$$P_{\mathrm{t}} = \left| \frac{t_1 t_2}{1 - r_1 r_2 e^{-\mathrm{i}\phi_{\mathrm{RT}}}} \right|^2 \tag{8}$$

Equation 8 can be simplified to:

$$P_{\mathrm{t}} = \frac{t_1^2 t_2^2}{1 + r_1^2 r_2^2 - 2 r_1 r_2 \cos\left(\phi_{\mathrm{RT}}\right)} \tag{9}$$

Now, equation 9 achieves a maxima whenever the round trip phase, ϕ_{RT}, is a multiple of 2π. The frequencies at which this happens corresponds to a resonant peak. Suppose ν_0 corresponds to a particular resonant peak frequency giving $\phi_{\mathrm{RT}} = 2k\pi$, for some $k \in \mathbb{Z}$. Equation 4 gives:

$$\frac{4\pi\nu_0 \mathrm{L}}{c} - 2N\phi_{\mathrm{G}} = 2k\pi \tag{10}$$

Now, consider the frequency of the laser, ν, to be ***extremely*** close to the resonant peak frequency ν_0.

$$\Rightarrow \frac{4\pi\nu \mathrm{L}}{c} - 2N\phi_{\mathrm{G}} = \phi_{\mathrm{RT}}$$

Subtracting equation 10 from the above gives us:

$$\frac{4\pi(\nu - \nu_0)\mathrm{L}}{c} = \phi_{\mathrm{RT}} - 2k\pi$$

$$\Rightarrow \phi_{\mathrm{RT}} = 2k\pi + \frac{4\pi(\nu - \nu_0)\mathrm{L}}{c}$$

Substituting this back into equation 9, we get:

$$P_{\mathrm{t}} = \frac{t_1^2 t_2^2}{1 + r_1^2 r_2^2 - 2 r_1 r_2 \cos\left(2k\pi + \frac{4\pi(\nu-\nu_0)\mathrm{L}}{c}\right)}$$

$$\Rightarrow P_{\mathrm{t}} = \frac{t_1^2 t_2^2}{1 + r_1^2 r_2^2 - 2 r_1 r_2 \cos\left(\frac{4\pi(\nu-\nu_0)\mathrm{L}}{c}\right)} \tag{11}$$

Now, as specified earlier, ν is ***extremely*** close to ν_0, i.e. $(\nu - \nu_0) \to 0$.

$$\Rightarrow \left(\frac{4\pi(\nu - \nu_0)\mathrm{L}}{c}\right) \to 0, \text{ for } \textit{appropriately} \text{ chosen } '\nu'$$

using the approximation, $\cos\theta \approx 1 - \frac{\theta^2}{2}$ in equation 11, we get:

$$P_t = \frac{t_1^2 t_2^2}{(1 + r_1^2 r_2^2 - 2r_1 r_2) + r_1 r_2 \left(\frac{4\pi(\nu-\nu_0)L}{c}\right)^2}$$

$$\Rightarrow P_t = \frac{t_1^2 t_2^2}{(1 - r_1 r_2)^2 + \left(\frac{4\pi\sqrt{r_1 r_2}(\nu-\nu_0)L}{c}\right)^2} \tag{12}$$

Equation 12 can be ***carefully*** re-written as follows:

$$P_t = \frac{a}{1 + \left(\frac{\nu-\nu_0}{b}\right)^2} \tag{13}$$

with

$$a = \left(\frac{t_1 t_2}{1 - r_1 r_2}\right)^2 \tag{14}$$

$$b = \frac{c(1 - r_1 r_2)}{4\pi\sqrt{r_1 r_2}L} = \frac{\nu_{FSR}}{2\mathcal{F}} \tag{15}$$

$$\nu_0 \rightarrow \text{Resonant Peak Frequency} \tag{16}$$

Equation 13 is the famous ***Lorentzian distribution***, and this is what we use as our *fitting model*. Equations 14, 15 and 16 are what we use to determine the physical cavity parameters using the ones given by the fitting procedure(viz. $'a'$, $'b'$ and $'\nu_0'$)

D Transfer Function Measurement

Transfer Function is a mathematical representation of the frequency response of system. In the frequency/Laplace domain, for a linear, time invariant system, it is simply given as the ratio of the output(Y) to the input(X), when the system is subject to continuous time input and output signals. Hence,

$$H(s) = \frac{Y(s)}{X(s)}$$

where $s = i\omega$ is the spatial frequency and $H(s) = \mathcal{L}\{h(t)\}$, $Y(s) = \mathcal{L}\{y(t)\}$ and $X(s) = \mathcal{L}\{x(t)\}$ are the Laplace transforms of the transfer function, output signal and input signal in the time domain respectively. The transfer function has essentially two physically relevant components, the magnitude/gain, $|H(s)|$, and phase, $\arg(H(s))$. We usually represent the frequency response of a system using a Bode plot, which consists of two plots, showing respectively the magnitude(dB) vs frequency(Hz) and phase(degrees) vs frequency(Hz) response. For details on electrical transfer functions and Bode plots, refer to [25].

For our purpose, we use the Network Analyzer, Agilent Technologies AG4395A([20]), to measure the frequency response transfer function of Photodetectors. As the Network Analyzer does not have a an in-built mechanism for measuring the standard deviation(error) in

the data for magnitude and phase, we also develop a python script to perform the measurement multiple times. We also develop a script for assessing the multiple sets of data obtained through the above script and report to us the mean magnitude and phase frequency response along with errors in a Bode plot. Both these scripts can be found at [26]. These error values are important because we would like to know how accurate and precise measurements and information we can obtain for the magnitude and phase frequency response. This will allow us to estimate the importance of points/regions where the transfer function varies rapidly due to noise sources. This is especially true when the magnitude gain is extremely low and the phase of the transfer function varies a lot.

The above assessment can also be extended by relating a quantity like *coherence* to the measurements. This part of the measurement still isn't that concrete and hence is left as it is for now.

D.1 Frequency Response Measurement for Photodetectors

The Photodetectors(PDs) that are to be used for conducting the experiments need to be quite sensitive and have a 'large' enough bandwidth. For our purpose, we would like to work with PDs with at least 30 MHz frequency bandwidth. In sections D.2 and D.3 , we'll determine the bandwidth of two PDs: ET-3040 and ET-3010. The PDs were bought from Electro-Optics Technology, Inc. To refer to their datasheets, see [18]. The schematic of the test is shown in figure 16. The laser used has wavelength $1064nm$. It is pumped using a current of 19.5 mA producing a power of 1.00 mW. In place of Detector Under Test(DUT), we put the ET-3040 or ET-3010 PDs. The reference PD is one of the New Focus Inc.'s High-Speed Photoreceivers, model 1611 with an DC transimpedance, $\mathbf{T}^{\text{ref}}_{\text{DC}} = 10\ \text{k}\Omega$ and an AC transimpedance, $\mathbf{T}^{\text{ref}}_{\text{RF}} = 700\ \Omega$. Its datasheet can be seen at [19]. The Network/Spectrum Analyzer shown is the Agilent Technologies AG4395A([20]). The procedure for testing both the PDs is similar. After allignment, we first observe readings for a DC source and then for an RF modulated signal. We then, using the Network Analyzer obtain data points for the modulated RF signal and then plot them to determine the approximate bandwidth of the PDs.

The network analyzer measures the tranfer function of the system in dB. Once we obtain the data points, we can calibrate the Bode plots with the transimpedance frequency response of the PD, considering that the ratio of the currents would remain the same in both the DC input as well as the RF modulated signal. The formula for that is given as:

$$\mathbf{T}^{\text{DUT}}_{\text{rf}} = \frac{H^{\text{DUT}}}{H^{\text{ref}}} \times \frac{\mathbf{V}^{\text{ref}}_{\text{DC}}}{\mathbf{V}^{\text{DUT}}_{\text{DC}}} \times \frac{\mathbf{T}^{\text{DUT}}_{\text{DC}}}{\mathbf{T}^{\text{ref}}_{\text{DC}}} \times \mathbf{T}^{\text{ref}}_{\text{rf}}$$

where $\mathbf{T}^{\text{DUT}}_{\text{rf}}$ and $\mathbf{T}^{\text{ref}}_{\text{rf}}$ are the 'rf' transimpedances of the test detector and the reference detector respectively, $\mathbf{T}^{\text{DUT}}_{\text{DC}}$ and $\mathbf{T}^{\text{ref}}_{\text{DC}}$ are the 'DC' transimpedances of the test detector and the reference detector respectively. $\mathbf{V}^{\text{ref}}_{\text{DC}}$ and $\mathbf{V}^{\text{DUT}}_{\text{DC}}$ are the measured 'DC' output potentials of the reference detector and the test detector respectively. The ratio $\frac{H^{\text{DUT}}}{H^{\text{ref}}}$ is obtained using the Network Analyzer. We will use this equation to determine the response characteristics of test detectors, particularly of the ones stated in sections D.2 and D.3. To learn more about the transimpedance calibration and its premise, refer to [21].

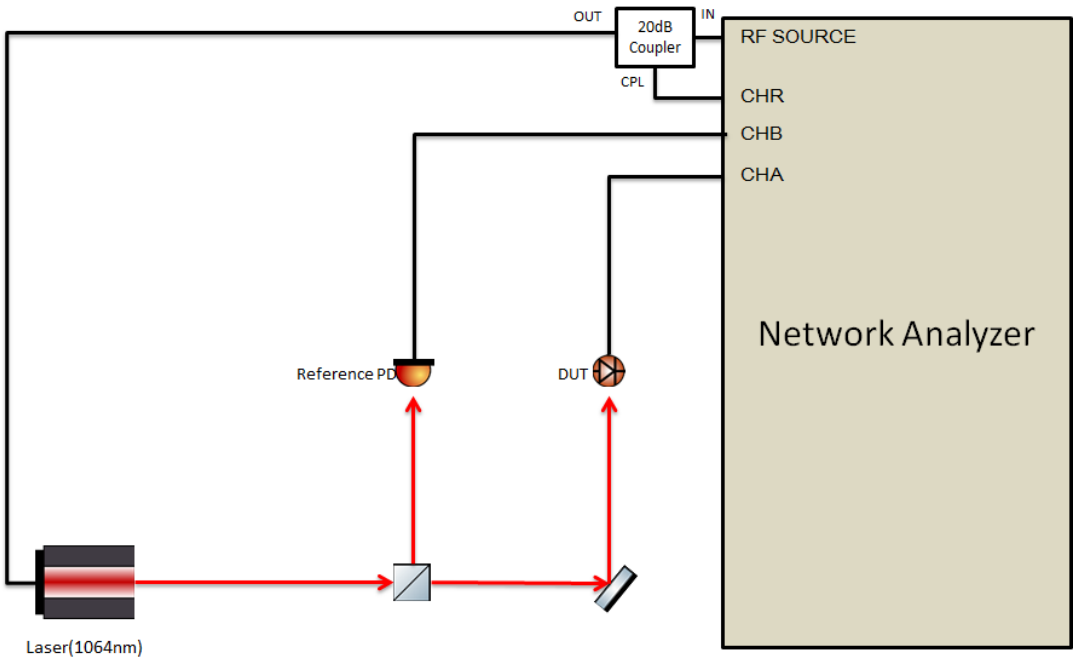

Figure 16: Schematic for Testing the PDs

D.2 ET-3040

For the DC measurement, we obtained the following values for the DC voltages for the ref PD and the DUT respectively:

$$\mathbf{V}_{\mathrm{DC}}^{\mathrm{ref}} = 1.8V$$

$$\mathbf{V}_{\mathrm{DC}}^{\mathrm{DUT}} = 15mV$$

Using the DC transimpedances of $\mathbf{T}_{\mathrm{DC}}^{\mathrm{ref}} = 10\ \mathrm{k}\Omega$ and $\mathbf{T}_{\mathrm{DC}}^{\mathrm{DUT}} = 50\Omega$ for the reference detector and the DUT respectively, we find the respective photocurrents in the two PDs to be:

$$\mathbf{I}_{\mathrm{DC}}^{\mathrm{ref}} = 180\mu A$$

$$\mathbf{I}_{\mathrm{DC}}^{\mathrm{DUT}} = 300\mu A$$

The responsivities, in A/W, for the reference detector and the DUT are given to be nearly 0.75 and 0.9 respectively. Using these we calculate the power in the two PDs:

$$\mathbf{P}_{\mathrm{DC}}^{\mathrm{ref}} = 240\mu W$$

$$\mathbf{P}_{\mathrm{DC}}^{\mathrm{DUT}} \approx 333.3\mu W$$

i.e. the fraction of the total power of the laser that went into the reference detector and the DUT, respectively, were 24% and 33.33%.

Using the Netwrok Analyzer, we obtained data points for an RF signal swept from 100 kHz to 500 MHz. The Bode plot for the ET-3040 PD in this sweep is shown in Figure 17.

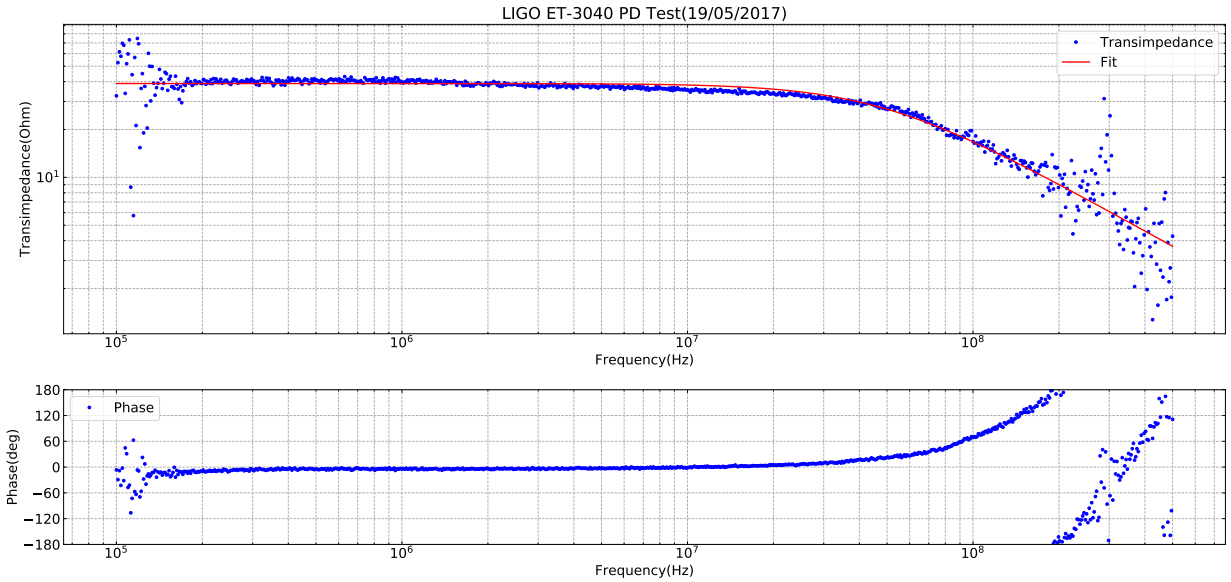

Figure 17: Bode Plot for PD ET-3040 in reference to High Speed Photoreceiver model:1611

D.3 ET-3010

The ET-3010 PD has an extremely small active area diameter of 100 μm. It requires a fiber coupled input for proper testing but we performed on it with an extremely low powered laser(1.00 mW). As the active area is so small, we used Stanford Research Systems' low noise voltage preamplifier, SR560 [22], to increase the votage output of these PDs by a gain of 100.

For the DC measurement, we obtained the following values for the DC voltages for the ref PD and the DUT respectively:

$$\mathbf{V}_{\mathrm{DC}}^{\mathrm{ref}} = 1.8V$$

SR560 offset voltage without detector signal = 120.6 mV
Voltage reading with detector signal = 348.6 mV
SR560 gain = 100

$$\mathbf{V}_{\mathrm{DC}}^{\mathrm{DUT}} = 2.28mV$$

Using the DC transimpedances of $\mathbf{T}_{\mathrm{DC}}^{\mathrm{ref}} = 10\ \mathrm{k}\Omega$ and $\mathbf{T}_{\mathrm{DC}}^{\mathrm{DUT}} = 50\Omega$ for the reference detector and the DUT respectively, we find the respective photocurrents in the two PDs to be:

$$\mathbf{I}_{\mathrm{DC}}^{\mathrm{ref}} = 180\mu A$$

$$\mathbf{I}_{\mathrm{DC}}^{\mathrm{DUT}} = 45.6\mu A$$

The responsivities, in A/W, for the reference detector and the DUT are given to be nearly 0.75 and 0.85 respectively. Using these we calculate the power in the two PDs:

$$\mathbf{P}_{\mathrm{DC}}^{\mathrm{ref}} = 240\mu W$$

$$\mathbf{P}_{\mathrm{DC}}^{\mathrm{DUT}} \approx 53.6\mu W$$

i.e. the fraction of the total power of the laser that went into the reference detector and the DUT, respectively, were 24% and 5.36%.

Using the Netwrok Analyzer, we obtained data points for an RF signal swept from 100 kHz to 500 MHz. The Bode plot for the ET-3010 PD in this sweep is shown in Figure 18.

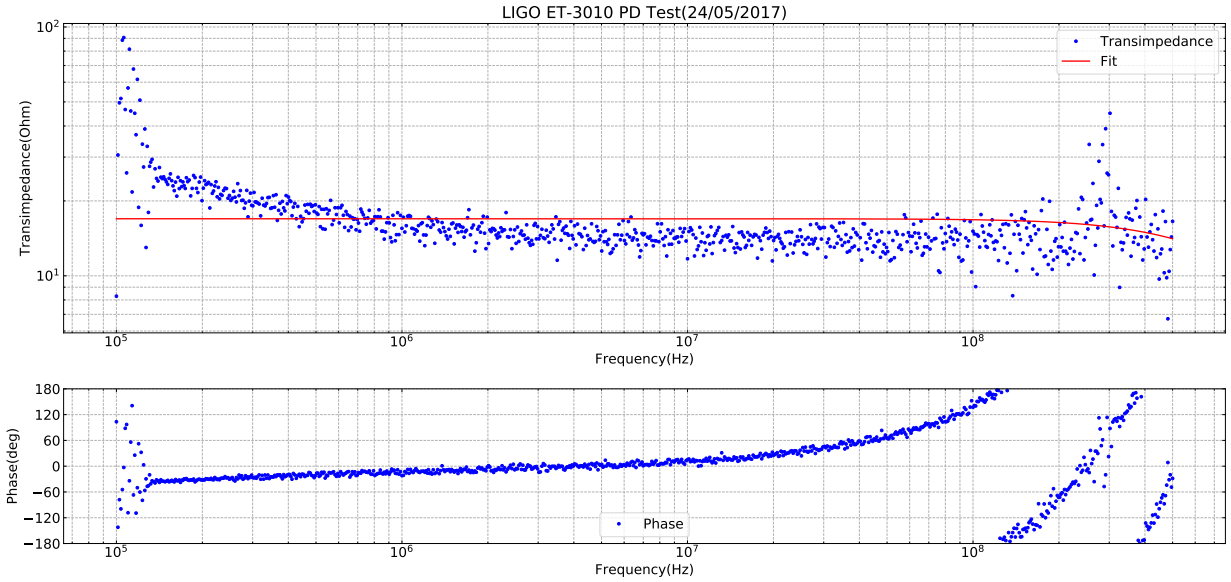

Figure 18: Bode Plot for PD ET-3010 in reference to High Speed Photoreceiver model:1611

References

[1] A. Einstein, *Sitzungsber Preuss. Akad. Wiss. 1, 688* (1916).

[2] A. Einstein, *Sitzungsber Preuss. Akad. Wiss. 1, 154* (1918).

[3] M. Maggiore, "Gravitational waves", Oxford University Press (2008).

[4] *40m Interferometer Image Src:* http://www.ligo.org/images/faq-ifo.png

[5] Joseph M. Geary, *Introduction to Optical Testing, SPIE Optical Engineering Press* (1993).

[6] Akito Araya, Souichi Telada, Kuniharu Tochikubo, Shinsuke Taniguchi, Ryutaro Takahashi, Keita Kawabe, Daisuke Tatsumi, Toshitaka Yamazaki, Seiji Kawamura, Shinji Miyoki, Shigenori Moriwaki, Mitsuru Musha, Shigeo Nagano, Masa-Katsu Fujimoto, Kazuo Horikoshi, Norikatsu Mio, Yutaka Naito, Akiteru Takamori, and Kazuhiro Yamamoto, *"Absolute-length determination of a long-baseline FabryPerot cavity by means of resonating modulation sidebands,"* Appl. Opt. 38, 2848-2856 (1999).

[7] N. Uehara and K. Ueda, *"Accurate measurement of the radius of curvature of a concave mirror and the power dependence in a high-finesse FabryPerot interferometer,"* Appl. Opt. 34, 5611-5619 (1995).

[8] R. W. P. Drever, J. L. Hall, F. V. Kowalski, J. Hough, G. M. Ford, A. J. Munley, and H. Ward, *Laser phase and frequency stabilization using an optical resonator*, Applied Physics B: Lasers and Optics 31, 97-105 (1983). 10.1007/BF00702605.

[9] Alberto Stochino, Koji Arai and Rana X. Adhikari, *A Technique for In-situ Measurement of Free Spectral Range and Transverse Mode Spacing of Optical Cavities.* LIGO DCC No. - P1200048 (https://dcc.ligo.org/LIGO-P1200048).

[10] Y. R. Shen, *The principles of nonlinear optics* (John Wiley, New York, 1984).

[11] R. W. Boyd, *Nonlinear Optics* (Academic Press, Boston, 1992).

[12] Kiwamu Izumi, Koji Arai, Bryan Barr, Joseph Betzwieser, Aidan Brooks, Katrin Dahl, Suresh Doravari, Jennifer C. Driggers, W. Zach Korth, Haixing Miao, Jameson Rollins, Stephen Vass, David Yeaton-Massey and Rana X. Adhikari, *Multi-color Cavity Metrology.* LIGO DCC No. - P1200019 (https://dcc.ligo.org/LIGO-P1200019).

[13] Andreas Freise and Daniel Brown, FINESSE(www.gwoptics.org/finesse). LIGO DCC No. - T1300431 (https://dcc.ligo.org/LIGO-T1300431)

[14] Tango, W.J. Appl. Phys. (1977) 13: 327. https://doi.org/10.1007/BF00882606

[15] Qian, S.S., Stow, C.A., Borsuk, M.E., 2003. On monte carlo methods for bayesian inference. Ecol. Modell. 159, 269277. https://doi.org/10.1016/S0304-3800(02)00299-5

[16] Naomi Wharton, Koji Arai and Rana Adhikari, *Laser Mode Spectroscopy for Mirror Metrology.* LIGO DCC No. - T1700196 (https://dcc.ligo.org/LIGO-T1700196)

[17] *Code to generate a simulation for the 40m Fabry-Pérot Cavity Scan plot can be found in the following git repository:* https://github.com/CaltechExperimentalGravity/ModeSpectroscopy[Folder:Cavity_Scan_Fitting]

[18] *Datasheets for ET-3040 and ET-3010 PDs:* http://www.eotech.com/13/user-guides/photodetectors/non-amplified-photodetectors

[19] *Datasheet for New Focus Inc.'s High Speed Photoreceiver 1611:* http://assets.newport.com/webDocuments-EN/images/15178.pdf

[20] *Datasheet for Agilent Technologies AG4395A Network Analyzer is on the 40m wiki:* https://wiki-40m.ligo.caltech.edu/Electronics/AG4395A?action=AttachFile&do=view&target=AG4395a.pdf[[attachment:AG4395a.pdf]]

[21] Alberto Stochino. *40m RF PDs Upgrade*. LIGO DCC No. - T1000209 (https://dcc.ligo.org/LIGO-T1000209).

[22] *Datasheet for Low Noise Voltage Preamplifier SR560:* http://www.thinksrs.com/downloads/PDFs/Manuals/SR560m.pdf

[23] Anthony E. Siegman, *Lasers*, 1986. University Science Books.

[24] *Internisty Profile of Lower Order TEM Modes Image Src:* https://www.rp-photonics.com/hermite_gaussian_modes.html

[25] Bakshi, V. U. B. U. A., *Control Systems*, 2007. Technical Publications

[26] *Code for performing multiple measurements using the AG4395A Network Analyzer and then assessing the data:* https://github.com/CaltechExperimentalGravity/ModeSpectroscopy[Folder:Network_Analyzer_Code]